# Reorientation of the Left Ventricular Long-Axis on Myocardial Transaxial Tomograms by a Linear Fitting Method

Zuo-Xiang He, Jean C. Maublant, Jean C. Cauvin, and Annie Veyre

*Service de Médecine Nucléaire, Centre Jean Perrin, Université d'Auvergne, Clermont-Ferrand, France; and Department of Nuclear Medicine, Cardiovascular Institute and Fu Wai Hospital, Chinese Academy of Medical Sciences, Beijing, China*

A method is described for reorientating the left ventricular (LV) long-axis from myocardial transaxial tomographic data. On a midventricular transverse slice and on a midventricular sagittal slice, the apical and basal limits are selected successively by the operator. The linear activity profiles between these two limits are plotted line by line. In each profile, the two points with the maximum counts in the septal and lateral walls on the transverse slice, or in the anterior and inferior walls on the sagittal slice, are detected. The intermediate point with the minimum counts is then determined. The set of points with minimum counts are fitted by a straight line using the least squares method. This line is taken as the LV long-axis. In a series of 15 cases with stress-delayed $^{201}$Tl SPECT, the reproducibility of the reorientation with this semi-automatic method was compared with manual selection of the LV long-axis. In all patients, a successful reorientation was obtained with the present method. The reproducibility was significantly better with the semi-automatic method than with the manual selection of the LV long-axis.

**J Nucl Med 1991; 32:1794–1800**

Thallium-201 myocardial SPECT is now widely accepted for the diagnosis of coronary artery disease (CAD), qualitative and quantitative evaluation of the extent and size of myocardial infarction and ischemia, as well as evaluation of myocardial viability (*1–8*). Anatomically, the main axis, or long-axis, of the left ventricle (LV) is rotated to the left and downwards, and the transaxial tomograms may not provide sufficient information about the anatomic relationship of the myocardial segments. Since the LV tracer distribution is grossly symmetrical when represented on short-axis sections, they have become the most popular way for displaying myocardial tomograms. Most of the quantitative analysis methods are based on this representation. This means that the LV long-axis has to be reorientated after the reconstruction of the transaxial sections. Usually, this is achieved by manual selection of the LV long-axis on the transaxial and sagittal sections (*11,12*). This procedure is sometimes difficult for the operator and the resulting reproducibility is poor. Recently, it was demonstrated that incorrect selection of the LV long-axis can produce significant artifacts and that the quantitative analysis can be misleading because of incorrect reangulation (*13,14*). Therefore, a more sophisticated, automatic method is necessary to obtain satisfactory oblique angle tomograms and reliable quantitative results.

Recently, a method for automatically centering brain tomograms was developed (*15*). Unfortunately, although some attempts have been made (*9*), an automatic method for myocardial tomography is still not yet available, probably because of its inherent difficulty due to geometrical assymetry of the cardiac spatial location and myocardial volume distribution.

We describe a semi-automatic nongeometrically-dependent method for LV long-axis reorientation of $^{201}$Tl myocardial tomograms and report its results in a preliminary clinical application.

## MATERIALS AND METHODS

### Theoretical Background

The LV shape can be approximated by an ellipsoid (*17*), whose long-axis is rotated to the left (horizontal angle, HA) (Fig. 1a) and downwards (vertical angle, VA) (Fig. 1e). To reconstruct oblique angle tomograms perpendicular to the LV long-axis or short-axis, the LV long-axis has to be reorientated, i.e., these horizontal and vertical angles must be defined and corrected. Presently, this processing is usually performed by manual selection of the LV long-axis, co-ordinate transformation and appropriate interpolation (*11*).

Mathematical morphology allows the image of an object to be transferred into its skeleton. This structure is a set of adjacent points (*18–20*). The skeleton of a midventricular transaxial slice is horse-shoe shaped with two curved sides, the septum and lateral walls. Therefore, the medial axis should be in the middle of the segment perpendicular to the medial axis and intercepting with both the septal and lateral walls.

Received Sept. 17, 1990; revision accepted Mar. 27, 1991.
For reprints contact: Zuo-Xiang He, MD, Service de Médecine Nucléaire, Centre Antoine Lacassagne, Université de Nice, 06054 Nice Cedex, France.

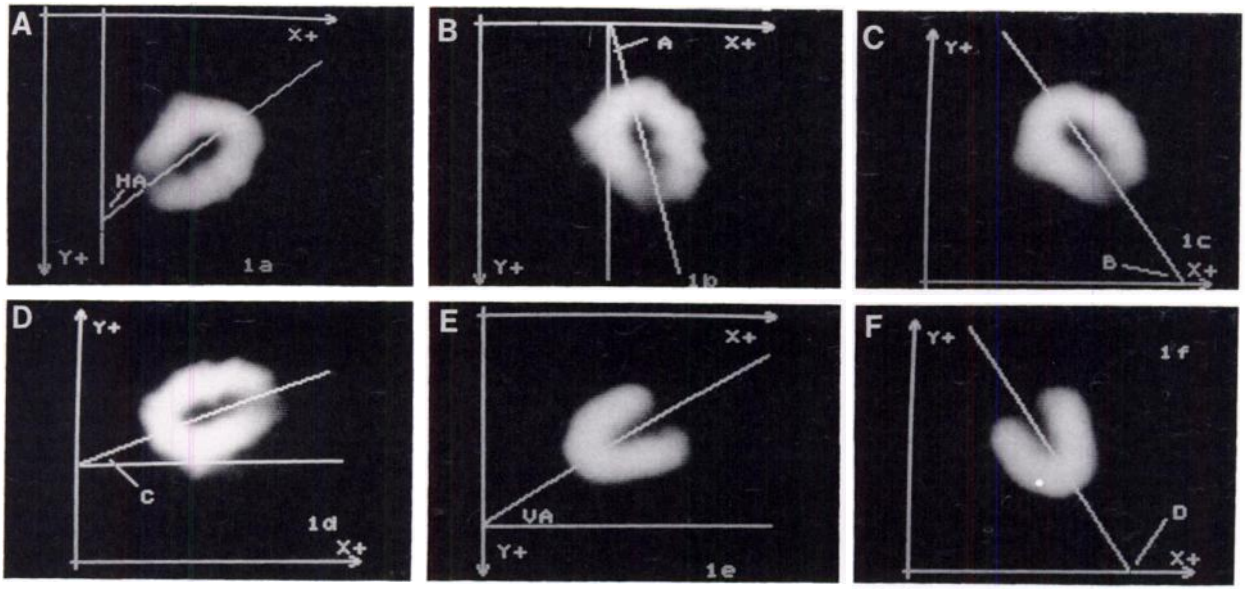


**FIGURE 1.** The angles between the LV long-axis and body principle axis (see text).

In practice, the media point is very difficult to define geometrically, but fortunately, a linear profile (ordinate-counts) can be easily obtained (Fig. 2c–d). On the profile, the two peaks with the maximum counts can be considered as representing the location of the LV septal and lateral walls on a transverse section (Fig. 2c) or as the anterior and inferior walls on a sagittal section (Fig. 2d). We postulate that the straight line fitted by the set of points with the minimum counts from the linear profiles on a midventricular slice approximates the LV medial or long axis.

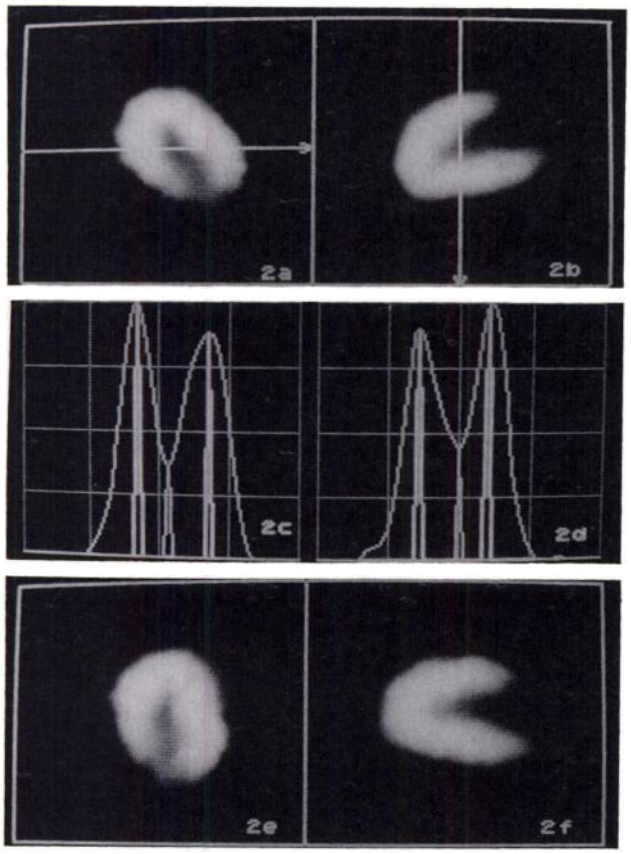


**FIGURE 2.** The creation of profile, the detection of the peaks and the nadir in profile, and the reorientation of the LV long-axis from transaxial and sagittal slices (see text).

### Data Acquisition and Reconstruction of Transaxial Tomograms

A series of 32 views (30–40 sec each) were acquired stepwise along a 180° arc extending from the right anterior oblique (RAO) to the left posterior oblique (LPO) projection. A large field of view scintillation camera equipped with a low-energy all-purpose collimator and interfaced to a dedicated computer were used for data acquisition. The energy window is set to 25%, centered on the 69–83 keV x-ray. All projections were acquired and stored as 64 × 64 × 16 bit matrices.

Transaxial tomograms are reconstructed using a routine filtered back projection algorithm with the Hamming/Hann filter. No attenuation or scatter correction were used.

### Reorientation of the Transaxial Sections and Reconstruction of the Sagittal Sections

The heart was manually centered, and the views were zoomed by a factor of 2.0 and interpolation. The values of the pixels out of 75% of the center of the images were set to zero.

To correct for the HA, the following procedure was used.

1. The midventricular slice (with largest cavity) was manually selected by the operator and 10% of the maximum counts were substracted from each pixel. The slice was then rotated counterclockwise by 67.5°, and the 64 × 64 matrix was interpolated to a 128 × 128 format (Fig. 1b, Fig. 2a).
2. The apical limit was set to the endocardial border of the LV apex and the basal limit was defined to the basal position of the LV by the operator. If, in these profiles, the peaks of activity representing to the myocardial walls and the nadir representing to the cavity could not be detected by the sequent algorithm, the operator was instructed to reset the limits.

3. For each line between the apical and basal limits, the linear profile was plotted, represented as coordinate versus counts (Fig. 2c). In each profile, the two peaks, respectively representing the septum and lateral walls, and the nadir, i.e., the point with minimum counts in the cavity, were automatically detected (*21*) (Fig. 2c).
4. The obtained set of points with minimum counts from each profile were fitted with the least squares method by a straight line (using $y = ax + b$, where a was the slope of the fitted line and b the intercept on the y-axis of the fitted straight line in the transferred coordinate).
5. The horizontal angle was calculated. Since a constructed midventricular transverse slice (Fig. 1a) was already rotated by 67.5° (Fig. 1b). In Figure 1b, A was the angle between LV long-axis and a line parallel to the y-axis, so:

$$HA = 67.5° - A.$$

The midventricular transaxial slice (Fig. 1a) and the rotated slice (Fig. 1b) were separately transferred to a new coordinate system (Fig. 1c–d), i.e., counterclockwise rotated by 90°. In Figure 1c, B is the angle between LV long-axis and the x-axis. In Figure 1d, C is the angle between the LV long axis and a line parallel to the X-axis. Therefore:

$$HA = B, \text{ and } A = C$$

We can then find the following equation:

$$HA = 67.5° - C.$$

From the previous procedures, we know b was the slope of the fitted straight line (Fig. 1d), $b = \text{Tan}(C)$, therefore, $C = \text{Tan}^{-1}(b)$. Therefore, the HA could be calculated according to the following equation:

$$HA = 67.5° - \text{Tan}^{-1}(b).$$

After obtaining HA, the transaxial slices were rotated counterclockwise by the calculated HA with appropriate interpolation (Fig. 2e).
6. The sagittal tomograms were reconstructed from these rotated transaxial slices.

For reorientating the LV long-axis in sagittal tomographic slices and reconstructing oblique angle tomograms, the algorithm is similar to that in transaxial slices. Briefly, the midventricular sagittal tomographic slice is selected by the operator, 10% of the maximum imaging counts are substracted from each pixel and both the apical and basal limits are set by the operator. For each line between the apical and basal limits, a profile is automatically created. The peaks, respectively representing the anterior and inferior walls and the nadir between the two peaks are detected (Fig. 2d). In sequence, the set of medial points with minimum counts on each profile are fitted by a straight line using the least square method.

The midventricular sagittal slice (Fig. 1e) is transferred to a new coordinate (Fig. 1f), i.e., rotated counterclockwise by 90°. In Figure 1f, D is the angle between LV long-axis and the x-axis, Therefore:

$$VA = D - 90°.$$

From the previous procedure, we know that b is the slope of the fitted straight line (Fig. 1f) ($b < 0$), $b = \text{Tan}(D)$, therefore, $D = \text{Tan}^{-1}(b)$. Therefore, the vertical angle can be calculated according to the following equation:

$$VA = \text{Tan}^{-1}(b) - 90°, \text{ or } VA = \text{Tan}^{-1}(\text{abs}(b)).$$

All the slices are rotated clockwise by the calculated vertical angle with appropriate interpolation (Fig. 2f). The rotated sagittal slices correspond to the vertical long axis tomograms. The horizontal long-axis and short-axis tomograms are reconstructed by the routine reconstruction algorithm.

### Preliminary Clinical Study

To evaluate the capability of the present method, it was applied to 30 myocardial tomographic studies of 15 consecutive patients who underwent routine stress and delayed $^{201}$Tl myocardial tomography (Table 1).

The results obtained with the method described above were compared with a manual selection of the LV long-axis. The reconstructed oblique angle tomograms were assessed by two experienced nuclear cardiologists. To test the reproducibility of the manual and present method, all procedures were performed by an experienced operator at two separate times. The rotated horizontal and vertical angles obtained by two methods were recorded. All procedures were repeated by another experienced operator and the rotated horizontal and vertical angles obtained by the two methods were recorded for analysis.

### Statistical Analysis

All data are presented as means and standard error of means (s.e.m.). The linear regression was applied to test the intra- and inter- observer reproducibility, the correlation coefficient (r) and standard error of estimate (s.e.m.) were determined. The significance of the correlation was tested by the F-ratio test. The difference of intraobserver and interobserver reproducibility studies are presented by the absolute value of the mean difference and standard deviation (s.d.). The differences between the paired data were tested by the paired t-test. Significance was assessed at the $p < 0.05$ level.

## RESULTS

A successful definition of the LV long-axis from the transverse and sagittal tomograms was obtained in all cases with the present method. The determined HA and VA with the manual selection of the LV long-axis and with the present method are summarized in Table 2. The differences in the determined HA and VA between the stress and delayed images of individual patients both by the present method and by manual selection of the LV long-axis are significant (Table 2).

### Intraobserver Agreement

For the determination of horizontal angle from the transaxial slice, the intraobserver agreement was excellent, $r = 0.99$ ($p < 0.001$) and $r = 0.98$ ($p < 0.001$) with the present method, while less satisfactory with the manual method, $r = 0.83$ ($p < 0.001$) and $r = 0.71$ ($p < 0.001$). s.e.e. values of the present method were lower than those with the manual selection of the LV long-axis (Table 3). The values of the horizontal angle by the present method were greater than with a manual selection of the LV long-axis.

**TABLE 1**
Description of the Patient Population (n = 15)

| Patient no. | Sex/Age | Location of defect* | Size of defect | Redistribution | Previous MI |
|---|---|---|---|---|---|
| 1 | M/67 | Ant, Sep, Ap | Large | + | no |
| 2 | F/31 | Inf | Medium | − | no |
| 3 | M/55 | Inf | Medium | − | no |
| 4 | M/58 | no defect | | | no |
| 5 | F/66 | Ap | Small | − | no |
| 6 | M/42 | Ant | Medium | + | no |
| 7 | F/67 | no defect | | | no |
| 8 | M/61 | Ap, Inf | Large | + | yes |
| 9 | M/56 | Inf | Large | − | no |
| 10 | M/40 | Inf | Large | − | no |
| 11 | M/59 | Inf | Large | − | no |
| 12 | M/61 | Ant, Inf | Medium | + | no |
| 13 | M/70 | Ap | Medium | − | no |
| 14 | M/42 | Sept, Inf | Medium + Large | + | yes |
| 15 | M/63 | Ap, Inf | Medium | − | no |

* Sept = septal; Ant = anterior; Ap = apical; and Inf = inferior.

For the determination of vertical angle from the sagittal slice, the intraobserver agreement was also good r = 0.99 ($p < 0.001$) and r = 0.98 ($p < 0.001$) with the present method, which improves slightly from the manual method, r = 0.92 ($p < 0.001$) and r = 0.92 ($p < 0.001$). But s.e.e. values of the present method were much smaller than with the manual selection of the LV long-axis (Table 3). The values of vertical angle by the present method was smaller than by a manual selection of the LV long-axis.

### Interobserver Agreement

For the determination of the horizontal angle in the transaxial tomographic slices, the interobserver agreement was excellent, r = 0.94–0.95 ($p < 0.001$) with the present method, while less satisfactory with the manual method, r = 0.70–0.83 ($p < .001$), and s.e.e.s were smaller with the present method (Table 4).

For the determination of vertical angle in the sagittal tomographic slices, the interobserver agreement was also excellent, r = 0.95–0.96 ($p < 0.001$) with the present method, while not as good with the manual method, r = 0.78–0.80 ($p < 0.001$) (Table 4).

## DISCUSSION

The technique presented in this paper provides a more reproducible reorientation of stress and redistribution myocardial tomograms than a manual method in a wide variety of defects. It can be advantageous to redisplay three-dimensional tomographic data in new orientations (*11*). Recently, re-orientation has also been used in brain studies (*15*). The advent of quantitative analysis of myocardial SPECT requires correct registration of the spatial

**TABLE 2**
Values of the Horizontal Angle (HA) and Vertical Angle (VA) Determined by Manual Selection of the LV Long-Axis (MS) and by the Present Method (PM) (n = 30) and the Differences in the Calculated HA (DHA) and VA (DVA) Between Stress and Delayed Imaging (n = 15)

| | HA | DHA | VA | DVA |
|---|---|---|---|---|
| MS | | | | |
| Operator 1A | 40.9 ± 0.7 | 3.9 ± 0.8† | 20.8 ± 1.9 | 6.1 ± 1.0† |
| Operator 1B | 41.4 ± 1.0 | 5.4 ± 0.9† | 18.7 ± 2.2 | 6.6 ± 1.2† |
| Operator 2A | 40.5 ± 1.4 | 6.4 ± 1.5† | 16.0 ± 1.8 | 3.3 ± 0.9* |
| Operator 2B | 38.3 ± 1.6 | 5.5 ± 1.0† | 13.9 ± 2.0 | 5.0 ± 1.0† |
| PS | | | | |
| Operator 1A | 48.7 ± 1.4 | 5.5 ± 1.4* | 14.4 ± 1.6 | 4.6 ± 0.8† |
| Operator 1B | 48.8 ± 1.4 | 5.3 ± 1.4* | 14.0 ± 1.6 | 4.7 ± 0.8† |
| Operator 2A | 47.9 ± 1.4 | 5.4 ± 1.3† | 14.0 ± 1.8 | 4.9 ± 1.0† |
| Operator 2B | 47.8 ± 1.4 | 5.2 ± 1.5* | 13.7 ± 1.8 | 5.9 ± 1.0† |

* $p < 0.01$.
† $p < 0.001$.
Operator 1 and 2 performed two measurements (A and B).

**TABLE 3**
Intraobserver Reproducibility of Operators 1 and 2 for Determination of the Horizontal Angle (HA) and Vertical Angle (VA) by Manual Selection of the LV Long-Axis (MS) and by the Present Method (PM) (n = 30)

| | | Difference (mean ± s.d.) | r | s.e.e. | Regression equation |
|---|---|---|---|---|---|
| HA | | | | | |
| Operator 1 | MS | 0.40 ± 3.89 | 0.72 | 3.96 | y = 0.689 + 0.896x |
| | PM | 0.10 ± 1.18 | 0.99 | 1.19 | y = 1.211 + 0.977x |
| Operator 2 | MS | 2.20 ± 4.80* | 0.83 | 4.80 | y = 1.994 + 0.986x |
| | PM | 0.03 ± 1.38 | 0.98 | 1.19 | y = 1.419 + 0.971x |
| VA | | | | | |
| Operator 1 | MS | 2.07 ± 4.88* | 0.92 | 4.92 | y = −3.257 + 1.057x |
| | PM | 0.33 ± 1.03 | 0.99 | 1.04 | y = 0.195 + 0.990x |
| Operator 2 | MS | 2.17 ± 4.11† | 0.91 | 3.82 | y = 0.567 + 0.830x |
| | PM | 0.30 ± 2.18 | 0.97 | 2.22 | y = −0.212 + 0.994x |

*$p < 0.05$.
†$p < 0.01$.

position of the heart. Of course, correct selection of the LV long-axis is essential.

It has been demonstrated that if the LV long-axis is selected incorrectly from either the transaxial or sagittal tomographic slices, the geometry of the reconstructed orthogonal slices can be distorted (*13*). Consequently, the sensitivity and the specificity of myocardial tomography could be lowered. Therefore, correct reorientation of the LV long-axis is of critical importance, and clinicians await the development of a more sophisticated, automatic and reproducible method.

Because of the assymmetry of the heart and of the myocardial tracer distribution, the automatic definition of the LV long-axis is difficult with a geometric method. The results of this study demonstrate that this can be successfully achieved with a nongeometric method.

### Disadvantages of Manual Selection of the LV Long-Axis

The limitations of manual selection of the LV long-axis have been recently recognized (*9,13*), although this method has been routinely used for several years (*10–12*).

**TABLE 4**
Interobserver Reproducibility for Determination of the Horizontal Angle (HA) and Vertical Angle (VA) by a Manual Selection of the LV Long-Axis (MS) and the Present Method (PM) (n = 30)

| | | Difference (mean ± s.d.) | r | s.e.e. | Regression equation |
|---|---|---|---|---|---|
| HA | | | | | |
| MS | Operator 1A-2A | 0.43 ± 5.03 | 0.83 | 4.49 | y = −24.587 + 1.591x |
| | Operator 1A-2B | 2.63 ± 6.16* | 0.73 | 5.89 | y = −23.831 + 1.518x |
| | Operator 1B-2A | 2.20 ± 4.80* | 0.70 | 5.70 | y = 0.328 + 0.970x |
| | Operator 1B-2B | 3.10 ± 5.52† | 0.76 | 6.15 | y = −9.403 + 1.152x |
| PM | Operator 1A-2A | 0.83 ± 2.74 | 0.94 | 2.73 | y = 2.722 + 0.927x |
| | Operator 1A-2B | 0.80 ± 2.48 | 0.95 | 2.45 | y = 2.830 + 0.926x |
| | Operator 1B-2A | 0.93 ± 2.43 | 0.95 | 2.44 | y = 1.493 + 0.950x |
| | Operator 1B-2A | 0.90 ± 2.34 | 0.95 | 2.33 | y = 1.975 + 0.941x |
| VA | | | | | |
| MS | Operator 1A-2A | 4.73 ± 5.37‡ | 0.86 | 5.06 | y = −0.776 + 0.809x |
| | Operator 1B-2A | 6.90 ± 6.88‡ | 0.78 | 5.69 | y = −0.060 + 0.671x |
| | Operator 1B-2A | 2.67 ± 6.27* | 0.85 | 5.78 | y = 3.023 + 0.696x |
| | Operator 1B-2B | 4.83 ± 7.46† | 0.79 | 5.63 | y = 2.929 + 0.585x |
| PM | Operator 1A-2A | 0.33 ± 2.76 | 0.96 | 2.72 | y = 1.463 + 1.079x |
| | Operator 1A-2B | 0.63 ± 3.10 | 0.95 | 3.05 | y = −1.921 + 1.090x |
| | Operator 1A-2A | 0.00 ± 2.85 | 0.96 | 2.82 | y = −1.091 + 1.078x |
| | Operator 1B-2B | 0.30 ± 3.00 | 0.96 | 2.94 | y = −1.659 + 1.097x |

*$p < 0.05$.
†$p < 0.01$.
‡$p < 0.001$.
Operator 1 and 2 performed two measurements (A and B).

This operator-dependent method relies on the operator's experience and is therefore subject to significant variability. In cases of significant myocardial abnormalities, it is difficult to obtain reproducible results with this method. In fact, in the present study, because of the large difference in the results from the two operators in the patients with large perfusion abnormalities, the slope of the regression line of the interobserver correlation was not satisfactory. However, it can be observed that the reproducibility of the manual selection of the LV long-axis from the sagittal slices was better than from the transaxial slices, which is related to the limited value of the vertical angle.

With such significant intra- and interobserver variabilities, the application of the manual re-orientation is limited, particularly for the comparison of stress and delayed myocardial tomography or myocardial tomography during interventions.

### Advantages and Potential Clinical Application of the Present Method

As determined by this preliminary study, our procedure has excellent reproducibility. The correlation coefficients of repeated studies were 0.98–0.99 (intraobserver), 0.94–0.95 (interobserver) for transaxial slices, 0.97–0.99 (intraobserver), 0.95–0.96 (interobserver) for sagittal slices. The intra- and interobserver differences of repeated studies were very small, and remained in a range that may be acceptable with the available imaging resolution.

Even in patients with large perfusion abnormalities, the LV long-axis was correctly defined by the present algorithm. In fact, if a 5% difference exists between the cavity and the point with maximum counts in myocardial wall, the point with minimum counts in the cavity can be correctly determined. In most circumstances, some degree of $^{201}$Tl uptake still exists in a transmural infarcted myocardium (*22,23*), and usually the radioactivity in the myocardial wall is higher than in the cavity.

Oblique angle tomography is the common technique in SPECT, PET, MRI and CT. Probably, the present method could be used in oblique angle tomographic reconstruction in myocardial PET studies. Recently, several approaches of the alignment of pairs of brain tomographic images have been developed (*25–27*). The correct registration of the myocardial tomograms may be carried out by the transformation of the LV long-axis.

Ideally, it would be desirable to compare the accuracy of reorientation by our method with a gold standard, but at present, no such standard is available. CT and MRI have a much higher spatial resolution, but the selection of the appropriate plan is difficult and the definition of the LV long-axis remains based on subjective or a priori criteria.

### Limitations

Some factors that may influence the accuracy of the present method should be noted. The accuracy of the definition of the LV long-axis is partly dependent on the quality of tomographic slices. This may be influenced by several physical factors (*16,28*). Particularly, the accuracy of the definition of the point with the minimum counts in profile is influenced by statistics of the low counts, although this effect is reduced by spatial filtering. In theory, the myocardial $^{201}$Tl uptake and the myocardial thickness (*16,24*) may have effects on the definition of the points with the minimum counts, but these effects don't seem very critical and is reduced by linear fitting.

Although that did not happen in our series, it remains possible that in some patients with abnormal cardiac location or morphology, the number of points found may be insufficient for a satisfactory linear fitting or that the straight line may not be satisfactory to describe the LV long-axis.

## CONCLUSION

This comprehensive, computerized method shows promise in providing a correct and reproducible method for reorientating and standardizing the LV long-axis and reconstructing oblique angle tomograms from transaxial tomographic data. More accurate quantitative analysis should be obtained with this method of reorientation than with a manual method. This method also makes it possible to correct three-dimensional registration of paired myocardial tomographies.


## ACKNOWLEDGMENTS

The authors wish to thank Dr. Jacques Darcourt and Pr. Françoise Lapalus from Centre Antoine Lacassagne, Faculté de Médecine, Université de Nice for their excellent suggestions and encouragement.


## REFERENCES


1. Pohost GM, Zir LM, Moore RH, et al. Differentiation of transiently ischemic from infarcted myocardium by serial imaging after a single dose of thallium-201. *Circulation* 1977;55:294–302.
2. Ritchie JL, Williams DL, Harp G, et al. Transaxial tomography with thallium-201 for detecting remote myocardial infarction. *Am J Cardiol* 1982;50:1236–1244.
3. Tamaki S, Najajima H, Murakami T, Yui Y, Kambara H, Kadota K. Estimation of infarct size by myocardial emission computed tomography with thallium-201 and its relation to creatine kinase-MB release after myocardial infarction in man. *Circulation* 1982;66:994–100.
4. Maublant JC, Cassagnes, J, Lejeune JJ, et al. A comparison between conventional scintigraphy and emission tomography with thallium-201 in the detection of myocardial infarction: concise communication. *J Nucl Med* 1982;23:204–208.
5. Tamaki N, Yonekura Y, Mukai T, et al. Stress thallium-201 transaxial emission tomography: quantitative versus qualitative analysis for evaluation of coronary artery disease. *J Am Coll Cardiol* 1984;4:1213–1221.
6. Depasquale EE, Nody AC, Depuey EG, et al. Quantitative rotational thallium-201 tomography for identifying and localizing coronary artery disease. *Circulation* 1988;77:316–327.
7. Maublant JC, Peycelon P, Cardot JC, Verdent J, Fagret D, Comet M. Value of myocardial defect size measured by Tl-201 SPECT: results of a multicenter trial comparing heparin and a new fibronlytic agent. *J Nucl Med* 1988;29:1486–1491.
8. Liu XJ, He ZX. Applications of myocardial scintigraphic imaging in cardiovascular diseases. *Chinese J Circ* 1989;4(suppl)236–243.
9. Cooke CD, Folks RD, Jones ME, Ezquerra NF, Garcia EV. Automatic program for determinating the long axis of the left ventricular myocardium used for thallium-201 tomographic reconstruction [Abstract]. *J Nucl Med*

1990;31:806.
10. Tamaki N, Yonekura, Y., Mukai T, et al. Segmental analysis of stress thallium myocardial emission tomography for localization of coronary artery disease. *Eur J Nucl Med*1984;9:99–105.
11. Borrello JA, Clinthorne NH, Rogers WL, Thrall JH, Keyes JW Jr. Oblique-angle tomography: a reconstructing algorithm from transaxial tomographic data. *J Nucl Med* 1981;22:471–473.
12. Garcia EV, Train KV, Maddahi J, et al. Quantification of rotational thallium-201 myocardial tomography. *J Nucl Med* 1985;26:17–26.
13. DePuey EG, Garcia EV. Optimal specificity of thallium-201 SPECT through recognition of imaging artifacts. *J Nucl Med* 1989;30:441–449.
14. Lancaster JL, Starling MR, Kopp DT, et al. Effect of errors in reangulation on planar and tomographic thallium-201 washout profile curves. *J Nucl Med* 1985;26:1445–1455.
15. Junck L, Moen JG, Hutchins, Brown MB, Kuhl DE. Correlation methods for the centering, rotation, and alignment of functional brain images. *J Nucl Med* 1990;31:1220–1226.
16. Hoffman EJ, Huang SC, Phelps ME. Quantitation in positron emission computed tomography. 1. Effect of object size. *J Comput Assist* 1979;3:299–308.
17. Blokland JAK, Vossepoel AM, Bakker AR, et al. Delineating elliptical objects with an application to cardiac scintigrams. *IEEE Trans Nucl Med* 1987;1:57–66.
18. Rosenfeld A. Axial representation of shap. *Comput Vision Graphics and Imagining Processing* 1986;33:156–173.
19. Serra J. *Imaging analysis and mathematical morphology, volume 1.* London: Academic Press, 1988:381–387.
20. Blum H, Nagel RN. Shape description using weighted symmetric axis features. *Pattern Recognit* 1978;10:167–182.
21. Coster M, Chermant SL. *Précis d'analyse d'images.* Paris: Editions du CNRS; 1985:373–375.
22. Watson DD, Smith WH, Lillywhite RC, Beller GA. Quantitative analysis of Tl-201 redistribution at 24 hours compared to 2 and 4 hours postinjection [Abstract]. *J Nucl Med* 1990;31:763.
23. Dilsizian V, Rocco TP, Strauss HW, Boucher CA. Technetium-99m-isonitrile myocardial uptake at rest. I. Relation to severity of coronary stenosis. *J Am Coll Cardiol* 1989;14:1673–1677.
24. Kojima A, Matsumoto M, Takahashi M, Hirota Y, Yoshida H. Effect of spatial resolution on SPECT quantification values. *J Nucl Med* 1989;30:508–514.
25. Faber T, Stokely E. Orientation of 3-D structures in medical images. *IEEE Trans Pattern Anal Mach Intel* 1988;10:626–633.
26. Alpert N, Bradshaw J, Kennedy D, Correia J. The principal axis transformation: a method for imaging registration. *J Nucl Med* 1990;31:1717–1722.
27. Pelizzari CA, Chen GTY, Spelbring DR, Weichselbaum RR, Chin C-T. Accurate three-dimensional registration of CT, PET, and/or MR images of the brain. *J Comp Assist Tomog* 1989;13:20–26.
28. Budinger TF. Physical attributes of single-photon tomography. *J Nucl Med* 1980;21:579–592.